Arctic Tundra Vegetation Functional Types Based on Photosynthetic Physiology and Optical Properties

Karl F. Huemmrich[a], John Gamon[b], Craig Tweedie[c], Petya P.K. Campbell[a], David Landis[d], Elizabeth Middleton[e]

[a]University of Maryland Baltimore County, Code 618, Goddard Space Flight Center, Greenbelt, MD 20771, USA, karl.f.huemmrich @ nasa.gov

[b]University of Alberta, Edmonton, Alberta, Canada

[c]University of Texas El Paso, El Paso, TX,

[d]Sigma Space Corp.,

[e]National Aeronautics and Space Administration

Abstract

Climate change in tundra regions may alter vegetation species composition and ecosystem carbon balance. Remote sensing provides critical tools for monitoring these changes as optical signals provide a way to scale from plot measurements to regional patterns. Gas exchange measurements of pure patches of key vegetation functional types (lichens, mosses, and vascular plants) in sedge tundra at Barrow AK, show three significantly different values of light use efficiency (LUE) with values of 0.013±0.001, 0.0018±0.0002, and 0.0012±0.0001 mol C mol^{-1} absorbed quanta for vascular plants, mosses and lichens, respectively. Further, discriminant analysis of patch reflectance identifies five spectral bands that can separate each vegetation functional type as well as nongreen material (bare soil, standing water, and dead leaves). These results were tested along a 100 m transect where midsummer spectral reflectance and vegetation coverage were measured at one meter intervals. Area-averaged canopy LUE estimated from coverage fractions of the three functional types varied widely, even over short distances. Patch-level statistical discriminant functions applied to in situ hyperspectral reflectance successfully unmixed cover fractions of the vegetation functional types. These functions, developed from the tram data, were applied to 30 m spatial resolution Earth Observing-1 Hyperion imaging spectrometer data to examine regional variability in distribution of the vegetation functional types and from those distributions, the variability of LUE. Across the landscape, there was a fivefold variation in tundra LUE that was correlated to a spectral vegetation index developed to detect vegetation chlorophyll content.

Introduction

High northern latitudes are undergoing dramatic changes in climate. Warming trends have been observed in northern regions and Global Circulation Model predictions indicate arctic and boreal regions are likely to warm by several degrees over the next century, a greater rate than other regions on the globe [1, 2]. Warming is particularly important in high latitude regions where seasonal shifts in surface properties involve freezing and thawing of water, so relatively small temperature changes around the freezing point can result in significant environmental shifts. Along with temperature changes, significant changes in precipitation and evapotranspiration are also predicted for these regions [1, 2].

Tundra vegetation is expected to be particularly responsive to climate change. Increased warming during the growing season is expected to alter production by lengthening the growing season and increasing metabolic activity [3, 4, 5]. Changes in seasonal air temperature may also result in changes in the depth of permafrost. This, in turn, can affect soil microbial activity, nutrient cycles and soil moisture [6, 7], which alter existing plant growth and competitive species interactions resulting in dramatic changes in vegetation composition. A unique characteristic of the tundra ecosystem is the relative dominance of non-vascular plants in the landscape, such as mosses and lichens. In some cases, mosses dominate local habitats in the tundra because of their tolerance to extreme cold, dessication, water-logging, and low light [8]. Lichens can survive extreme climate conditions such as drought and persistent freezing [9, 10, 11]. Tundra warming manipulation experiments have shown a decline in lichens with an increase in vascular plants [12].

Remote sensing is an important tool in the evaluation of ecosystem change as it provides repeatable and consistent measurements that can be collected over large expanses of the Earth. The difficulties in working in remote tundra locations have always incurred large logistical costs, therefore observation of ecosystem change rely on remote sensing as the most expedient and cost-effective way to collect information. Importantly, most remote sensing theory of vegetation has been derived from studies focused on temperate crops and forests and thus the interpretation of conventional remote sensing tools is often ambiguous for northern landscapes. There are several unique features of the tundra that affect the interpretation of remotely sensed data [13]. For example, non-vascular plants (mosses and lichens) may represent significant fractions of the tundra landscape cover, and these non-vascular plants have different physiological responses as well as different spectral characteristics from vascular plants or from bare soils [14, 15, 16]. Remote sensing studies have been able to detect changes in lichen-dominated areas due to responses to both short-term temperature anomalies as well as long-term temperature trends [17, 18].

This study investigates the importance of non-vascular plants to the tundra carbon balance and examines the use of spectral reflectance to distinguish these different functional types, using the concept of "optical types" to scale from ground-based *in situ* measurements to regional areas using satellite observations to examine vegetation functional type patterns across the tundra [19].

Materials and Methods

Study Area

The study area is a region mainly located north and west of the town of Barrow, AK, including most of the Barrow Environmental Observatory. Specific study plots are located at 71° 19' 19.1" N 156° 36' 15.9" W, approximately six miles east of Barrow. The area is classified as moist acidic coastal tundra [20]. Barrow has a mean annual temperature of –12.0°C, with a minimum mean monthly temperature of –26.6°C in February and maximum mean monthly temperature of 4.7°C in July. More than half of the 106 mm of annual precipitation falls as rain during a 3-month period from July through September, with the ground being snow covered from September through May to mid-June [21].

The tundra community at Barrow, AK consists of an overstory dominated by vascular plants (mostly graminoids) and an underlying mat of mosses [22]. Vascular plants at Barrow include dwarf shrubs, forbs, and perennial herbs but the most dominant growth form is graminoid [20]. Common vascular species are: *Carex aquatilis, Dupontia fischerii, Eriophorum angustifolium, E. scheuzerii, Luzula confusa, Petasites frigidus, Potentilla hyparctica,* and *Salix rotundifolia*. Mosses are a significant portion of the community and in some areas may account for more biomass than vascular plants [23]. Moss species include: *Dicranum elongatum, D. undulatum, Drepanocladus revolvens, Polytrichum (juniperum),* and *Sphagnum* spp. Lichens are scattered throughout the drier areas but are not as abundant or productive as mosses and graminoids [24] and include the species: *Alectoria nigricans, Cetraria cucullata, C. nivalis*, and *Dactylina arctica*.

Measurements

This project included: 1) the collection of *in situ* measurements of plots for the three vegetation functional types, including photosynthesis and spectral reflectance; 2) measurements at every meter along a 100 m transect of ground cover amount and spectral reflectance; 3) development of relationships between spectral reflectance and both photosynthesis and cover amount; 4) estimation of LUE across a tundra transect; and 5) application of these findings to the spectral information collected from Hyperion.

Vegetation measurements were designed to relate photosynthetic rate to spectral reflectance. Tundra vegetation was grouped into three functional categories; vascular plants, mosses, and lichens, with at least four replicates per group measured on any one day. Each replicate provided a different species from each group in an attempt to measure the variability within a group. Field sampling for this study was conducted on July 20 and August 5, 2001, near the peak of the growing season for this region.

Spectral reflectance measurements were collected at 51 plots, each about 15 cm in diameter, representing nearly pure areas of representative tundra species. Photosynthetic gas exchange measurements were collected at 17 of the plots. All of the study plots were in very close proximity (<15 m) to a 100 m linear transect that was also optically sampled at frequent intervals throughout the summer [25].

CO_2 gas exchange was measured at 17 plots where a 14.6 cm diameter collar of acrylic plastic was embedded in the ground. When measurements were made the plot was enclosed in a clear acrylic chamber constructed of 0.3175 cm thick acrylic tube glued to a 0.635 cm thick acrylic top and a closed gas exchange system was connected to the chamber (LI-6200, LiCOR, Lincoln, NE). Each individual plot was measured under ambient environmental conditions for net photosynthesis and then the measurement was

repeated after being covered with a black cloth to estimate dark respiration. Gross photosynthesis was calculated as the difference between the net photosynthesis, measured with the clear chamber, and dark respiration, measured with the chamber covered. A quantum sensor mounted on the chamber top measured incident photosynthetically active radiation (PAR). The chamber had a PAR transmittance of 95% [26]. Photosynthetic light-response curves were determined using household window screen material as neutral density filters to control incident PAR. This allowed photosynthesis measurements to be made for each functional type under a range of light levels.

Light use efficiency (LUE) was determined as the ratio of absorbed light and gross photosynthesis:

$$\varepsilon = \frac{G}{f_{PAR} Q_i} \quad (1)$$

where ε is LUE, G is gross photosynthesis with units of μmol CO_2 m^{-2} s^{-1}, Qi is incident PAR with units of μmol photons m^{-2} s^{-1}(i.e. photosynthetic photon flux density, or PPFD) and *f*PAR is the fraction of the PAR absorbed by the vegetation (unitless). Absorbed PAR (APAR) is the product of *f*PAR and incident PAR.

*f*PAR is not well defined and difficult to determine for vegetation with growth forms like lichens and mosses. We assumed that no PAR was transmitted through moss and lichen mats, so for these vegetation types *f*PAR is 1-PAR albedo. PAR albedo is estimated by integrating the measured spectral reflectance (see below) between 400 and 700 nm. For the vascular plant plots *f*PAR is determined using the linear relationship

between Normalized Difference Vegetation Index (NDVI) and *f*PAR described in Huemmrich et al. [26].

Optical Sampling

The optical field sampling consisted of measurements of the small single species plots, as well as measurements collected at every meter along a 100 m transect to observe areas of mixed coverage [25]. Optical measurements were collected using two portable field spectrometers (UniSpec, PP Systems, Haverhill, MA). These spectrometers measured reflectance between 310 and 1130 nm sampling at approximately 3 nm intervals.

For plot measurements, the spectrometer was fitted with a glass fiber optic cable connected to a stainless steel ferrule, which provided a 20° field of view. Reflected irradiance measurements were collected with the end of the fiber optic cable held vertically between 30 and 40 cm above the surface to view an area of less than 15 cm diameter to match the area of gas exchange measurements. Within seconds of collecting a surface measurement, a reference measurement was made of a calibration panel (Spectralon, Labsphere, Inc. North Sutton, NH). The speed of this procedure allowed the acquisition of data even under cloudy conditions. Three reflectance spectra were collected for each sampled plot, and were averaged to produce one spectrum per plot. In addition to the vegetation plots, spectral measurements for nongreen materials including bare soil, open water, and areas of standing dead vascular plants, were collected soon after snowmelt and before the start of green-up. For the vegetation plots, ground-based spectral reflectance measurements were collected near the height of peak productivity

period in early August (August 5 and 8, 2001) and reflectance for nongreen plots were collected throughout the summer (June 20 and 30, July 15, August 8 and 22, and September 3, 2001).

To characterize spectral reflectance patterns at multiple spatial scales, spectral measurements were made at 1 m intervals along a 100 m linear track system [25, 27]. The track was supported less than a meter above the tundra surface by tripods with a tram cart riding on the track carrying a dual channel spectroradiometer (Unispec DC, PP Systems). From the spectrometer were two fiber-optic cables mounted on a mast and boom attached to the cart, one attached to a diffuser head viewing upward, the other on the boom pointing vertically downward to view an area south of the track with a field-of-view of approximately 1 m in diameter. With each measurement of reflected radiance, a measurement of incident irradiance was also acquired at the same time for a determination of surface reflectance. Due to the coincident measurements of both incoming and reflected radiation this system was able to correct for effects of varying cloud cover. The tram system collected spectral measurements throughout the growing season that were repeatable while minimizing disturbance to the tundra surface [25, 27]. In this study we used measurements from the peak of the growing season period collected on August 10, 2001.

Processing the ground-measured spectral reflectance data included interpolating the spectral bands to 1 nm intervals. Due to instrument noise at the ends of the spectrometer range, the usable spectral range was between 400 and 1000 nm. The processing used freely available software (Multispec v.4.0, http://specnet.info/specnet_toolkit.htm). The spectral reflectance data were then

convolved to match the approximately 11 nm band passes of the Hyperion instrument [28] in subsequent analyses.

Regional imaging spectrometer data were acquired on July 20, 2009 (day 201) by the Hyperion instrument on the Earth Observing-1. Hyperion provides data in 220 spectral bands from 0.4 to 2.5 μm at 30-meter resolution and a 7.5 km wide swath [28]. The satellite data were atmospherically corrected to surface reflectance using the Atmosphere Removal algorithm (ATREM) [29, 30]. In this analysis, to match the spectral range of the ground-based spectral data, only 55 of the continuous Hyperion bands between 437 and 993 nm were used.

Discriminant analysis (DA) is a statistical technique for separating groups based on measured characteristics [31]. DA was used to develop functions separating the functional groups based on optical properties, determining the important spectral bands and simplifying the number of independent variables. The plot data were divided into four groups: vascular plants, mosses, lichens, and nongreen materials (bare soil, dead vegetation, and standing water). DA was applied to all the plot reflectance spectra convolved to the Hyperion bands using Systat (Version 13, Systat Software, Inc., Chicago, IL), using a forward stepwise method (Wilks' Lamda) to test for significant mean DA differences; a probability of $F \leq 0.05$ will pick the band but an $F \geq 0.10$ will remove the band.

At each meter along the 100 m transect a visual estimate of species abundance was made over the period August 8-11, 2001 using a 1 m by 1 m quadrat. The species data were converted into percent area of each of the vegetation functional types and nongreen material types. We estimate errors in the estimation of coverage to be +/- 15%

cover. Because of the three dimensional structure of the vegetation the sum of the coverage was more than 100%. For this analysis, the total measured cover values were normalized so total cover equals 100%.

LUE was determined for areas with mixtures of different functional types as the weighted sum of the LUE from the pure plots, where the weight coefficients were the normalized fractional cover values. This calculation assumes that the incident PAR is absorbed by the landscape components proportional to their normalized cover fraction and was applied to determine LUE for both the transect data and the Hyperion satellite imagery.

Chlorophyll concentrations are a key physiological factor related to maximum photosynthetic rates. We estimated chlorophyll concentrations using a semianalytical three-band model with the form:

$$C_i = [R(\lambda 1)^{-1} - R(\lambda 2)^{-1}] R(\lambda 3) \quad (2)$$

where the spectral index Ci is proportional to the chlorophyll concentration, and R(λ) is the reflectance for a given wavelength band, λ. Wavelengths chosen are maximally sensitive to absorption by chlorophyll and other pigments (λ1=549 nm), are influenced primarily by non-chlorophyll pigments (λ2=793 nm), and where reflectance is controlled by leaf scattering (λ3=793 nm) [32, 33, 34]. Vegetation functional type cover estimates retrieved from the Hyperion imagery were used to calculate regional LUE patterns. LUE per pixel was compared with chlorophyll estimates obtained with Equation 2.

Results

The physiological measurements identify differences relating to photosynthetic carbon exchange among the three vegetation functional types. From the plot gas exchange data, LUE for each functional type was calculated as the slope of a linear regression between gross photosynthesis and APAR, forced through the origin (Figure 1, Table 1). Lichens, mosses, and vascular plants all had different LUE values. Vascular plants had significantly higher net photosynthetic rates and LUE than the other two functional types. The vascular plant LUE from this study (0.0134 mol C mol^{-1} quanta) was close to that previously determined for a vascular plant overstory near Barrow (LUE=0.0126 mol C mol^{-1} quanta) and within the 95% confidence interval of the slope from the regression in this study (i.e. the vascular plant LUE). This was noteworthy as the LUE in this study was based only on measurements collected during the middle of the growing season, while the Huemmrich et al. [26] LUE was derived from measurements collected throughout the growing season, suggesting the LUE for vascular plants was relatively stable over much of the season.

The LUE for mosses and lichens were much lower than for vascular plants, however there was a significant difference between these two functional types as well (Table 1) with mosses having a LUE almost 50% greater than lichens (a similar analysis for LUE of the moss data was presented in [26]).

The *in situ* spectral reflectance measurements of the plots were divided up into four groups: vascular plants (n=22), mosses (n=11), lichens (n=18), and nongreen material (n=19) (Figure 2). Generally, the vascular plant and moss spectra were similar, and display typical green plant spectral reflectance patterns, including more variation in the near infrared than in visible wavelengths. In comparison, lichen spectra had much

higher visible reflectance and were more variable in all wavelengths. Spectral patterns for the nongreen materials were clearly different for dead vegetation, bare soil, and water. Generally the spectral variability for the entire nongreen group increases as a function of wavelength.

DA provided an objective tool to evaluate the ability of optical sampling to distinguish functional groups and to identify a subset of the spectral bands to do this separation. The stepwise method for DA reduced the number of wavebands from 55 to five, yet retained separation of functional types. The five chosen bands were located in key locations of typical green plant spectra (Figure 2); at the blue (488 nm) and red (671 nm) chlorophyll absorption wells, near the inflection point of the red edge (712 nm), at the shoulder of the red edge (763 nm), and in the near infrared "plateau" (834 nm). Mulhern [35] identified the blue band as an important spectral region for separating lichens from soils. The DA functions (Figure 3) correctly predicted 83% of group membership overall, with 86% correct for vascular plants, 91% for mosses, 95% for the nongreen materials, and 61% for lichens. Lichen errors were mainly due to confusion with the nongreen materials (Figure 3).

Even at the scale of one square meter, the cover estimates along the tram transect show that all square meter plots consisted of mixtures of multiple cover types (Figure 4). The observed cover estimates included little bare ground with maximum coverage of 20%, while standing dead vegetation ranged from 0-70%, and water from 0-100%. Moss coverage ranged from 0-100%, but when normalized to a 100% maximum total coverage maximum moss coverage was 40% +/- 7%, based on the propagation of an assumed 15% error in the original observations. Lichen coverage ranged from 0-90% with 35% +/- 7%

maximum normalized lichen coverage. Vascular plant coverage ranged between 40-150%, with normalized coverage of 18-88% +/- 9%. Microtopography was an important factor in determining the distribution of the different vegetation functional types. Vascular plant coverage was highest in the locally low areas, particularly the areas with standing water, while moss coverage was highest in locally low areas without standing water and on the edges of the wet areas. Lichen coverage was highest in the locally high areas where bare soil patches also occurred.

The DA technique applied to reflectance data can successfully separate the different vegetation functional types. However, the transect coverage observations indicate how heterogeneous the tundra is, as areas over a few square centimeters in size generally consist of mixtures of multiple types. Therefore, the fractions of each functional type within a 30 m Hyperion pixel are required to determine its overall LUE. We used the optical measurements to scale plot-level LUE to 30 m areas. Since the DA functions optimized separation of the different functional types with a small number of spectral bands, we used the distance to endmembers in the DA function space to estimate cover fractions in mixed pixels. Assuming that the range of *in situ* plot reflectances provide a reasonable description of the variability of plot type, the endmembers for the moss, lichen, and nongreen cover types were the average of the plot reflectances. However, variability in the vascular plants reflectance is driven by differences in green leaf area index. To account for that variability the vascular plant endmember was chosen to be the "greenest" plot spectra (i.e. the highest NDVI and was the greatest distance from the average of all the plot values in the DA function space).

Endmember reflectance for each functional type and reflectances at each meter along the transect were transformed using the DA functions. The distances in the DA space between the coverage estimates for each square meter and the endmembers were calculated, these were related to the observed coverage to create transfer functions. The statistical associations distance from endmembers and observed coverage along the transect were low due to observation errors that were large relative to the range of values, with R^2 values of 0.39, 0.13, and 0.19 for vascular plants, mosses, and lichens respectively. Nevertheless, the cover fractions determined from the *in situ* reflectance were found to be in close agreement with sampled cover fractions (Figure 6), with root mean square error (RMSE) of 11% cover for vascular plants, 8% for moss, 9% for lichen, and an overall RMSE of 9% cover.

LUE along was calculated for each square meter block along the transect using the observed cover fraction and coverage estimated from the reflectance spectra (Figures 5 and 7). Along the transect LUE was quite variable, with maximum and minimum values occurring within 6 m of each other (Figure 7). Variability in LUE was affected by microtopography, with higher values of LUE tending to occur in locally low, wet areas. This variability over the 100 m distance produced a fourfold difference in LUE with values from 0.003 to 0.012 mol C mol^{-1} quanta for the *in situ* observations. The average errors for estimating LUE were similar for the two methods: 0.0014 mol C mol^{-1} quanta for the method using observed coverage and 0.0015 mol C mol^{-1} quanta for the LUE based on the remote sensing approach. The two different LUE calculations have a correlation of 0.62 with a RMSE of 0.0013 mol C mol^{-1} quanta.

The equations relating spectral reflectance and functional type coverage derived from the transect data were applied to the Hyperion image to create a continuous fields description of the Barrow region (Figure 8b). Over this area the distribution of vascular plant coverage per pixel had a maximum value of 74% with a distribution peak of 32%, for mosses the regional maximum coverage was 31% with the distribution peak at 22%, and for lichens the maximum coverage was 22% with a peak of 10%. While we do not have independent data to evaluate these results, we got a sense of the accuracy of the coverage estimates by looking at coverage estimates in an area known to be free of vegetation, the old Naval Arctic Research Laboratory airfield. For the pixels of the runway vascular plant coverage was as high as 9%, moss 14%, and lichen 13%, which were close to the values of the RMSE found in the tram analysis. This consistency suggests that the method captures the actual functional type distribution within this range of error.

There are clearly observed spatial patterns in the cover fractions with high vascular plant coverage found on the margins of drained lakes, although not in the middle of the drained lakes, that often contain some standing water, while higher lichen coverage tended to be found in the drier upland regions, a pattern also observed along the transect (figure 4). Moss coverage was more widely distributed, although high moss coverage in the middle of the drained lakes may be erroneous because of confusion with mixtures of water and vascular plants. Field observations confirm that moss often occurs as a low, "background" layer beneath the vascular canopy of wet tundra in this region [26].

The Hyperion coverage estimates were used to calculate regional LUE patterns (Figure 8c). For the vegetated parts of the scene, the LUE ranged from 0.0021-0.0102

mol C mol^{-1} quanta, a fivefold difference between maximum and minimum LUE. The distribution peak of LUE for the region and the overall regional average were both 0.0048 mol C mol^{-1} quanta.

The Hyperion-based LUE was compared with the chlorophyll spectral index, Ci (Equation 2). Ci was well correlated with LUE over the study area (R^2=0.69, SE=0.0006 mol C mol^{-1} quanta) suggesting vegetation chlorophyll concentration is a key determinant of LUE for this tundra ecosystem (Figure 9). This suggests a more direct approach for deriving spatial patterns of LUE for tundra from imaging spectrometry based on a simple reflectance-based metric of chlorophyll.

Discussion

This study uses the concept of optical types [19] to examine a key characteristic of ecosystem carbon exchange in the tundra. To have usable optical types one must be able to identify significant functional differences in vegetation types, and spectrally identify the different types. Our grouping of tundra vegetation (vascular plants, mosses, and lichens) meets these criteria. Among the different types, the plot measurements showed distinct differences in LUE, a key variable describing photosynthetic carbon uptake and DA showed that the types could be separated based on their spectral reflectance. The ability to link LUE to reflectance characteristics provides an approach to scale from the ground measurements to regional distributions. Using an unmixing approach we were able to create continuous fields of key tundra functional types for the region, an improvement over simple classifications. Results from this study demonstrated how, even at the 1 m^2 plot scale, variable mixtures of functional types produced

significantly different values for LUE. Unmixing using spectral reflectance provides a unique estimate of LUE for each pixel. Remote sensing then provides a way to map large areas and make noninvasive repeat measurements to monitor ecosystem change. Remote sensing is particularly important tool for observing tundra due to the difficulties and expense involved in traveling to and working in this region, rendering direct field sampling over large areas impractical.

The correlation between LUE calculated from coverage estimates and the chlorophyll index (Ci), even though they use different algorithms and spectral bands, demonstrates how multiple approaches yield similar results. This convergence is most likely due to plant physiological constraints indicating chlorophyll concentration is a controlling factor in vegetation photosynthetic efficiency, and may provide a more direct approach to deriving LUE.

This study found significant variability in LUE at local scales (meters) in the field data collected along the transect and at regional scales (km) in the satellite imagery. This spatial variability is not accounted for in existing carbon flux models. Spatial distributions of vegetation functional types was strongly related to surface hydrology and thus to the surface microtopography, where elevation variations of a few centimeters may be significant. These results suggest that climate change affecting surface hydrology [36] will also affect spatial patterns of vegetation distribution and ecosystem carbon exchange. Particularly in a scenario of modified surface hydrology, we can expect that climate change will affect relative coverage due to differing responses of each of the types to climate change, and that these changes in cover will be associated with altered carbon balance.

The field measurements in this study collected only visible and near infrared spectral bands. Since hydrology is an important factor determining the vegetation functional type coverage, shortwave infrared bands should provide additional information on vegetation water content [37]. Recent observations combining NIR and blue bands to detect standing water in coastal tundra [38] may also prove useful at detecting hydrological changes linked to cover type and LUE.

Further field studies are required in other parts of the tundra biome to test and extend the results of this study and evaluate the ability to generalize the results. For example, shrubs are an important component of the tundra biome, although they do not represent a significant cover type in our study region and so were not explicitly included in this study. Shrub coverage has been shown to be increasing in the tundra [39], future work needs to examine their optical and physiological characteristics to see if they comprise an optically distinct cover type.

The use of multiple narrow spectral bands for the umixing points to an application for the future NASA Hyperspectral Infrared Imager (HyspIRI) mission for mapping tundra vegetation distribution according to physiological function, hydrology, and microtopography over the entire biome. The concept of optical types (optically distinguishable functional types) may prove to be useful for this kind of functional mapping. Similarly, simple metrics of surface water cover (e.g. [38]) or pigment distribution (e.g. [34]) may provide insight into the proximal causes of functional change in tundra ecosystems.

Conclusions

The close linking of optical properties and carbon flux measurements in this study has provided insights into the functioning of the tundra ecosystem by identifying fine-scale patterns of LUE related to hydrology and microtopography. This study also illustrates new "scaleable" functional mapping techniques that can be extended through the use of satellite remote sensing to larger regions. This approach lends itself to future studies considering how species composition relates to changing ecosystem function and provides a framework for studying ecosystem change through remote sensing that considers shifts in hydrology, species composition, and their effects on carbon balance.

Acknowledgements

Funding for the field component of this study was provided by IARC to J. Gamon and K.F. Huemmrich through the Desert Research Institute, Reno, Nevada. The authors thank Stan Houston and Erika Anderson for their work on the field data collection. Thanks also to Glen Kinoshita, Hyojung Kwon, Rommel Zulueta, Joe Verfaillie, and Bob Hollister for their help and friendship in the field; and the staff of BASC (Barrow Arctic Science Consortium) for logistics support.

References

[1] ACIA, *Impacts of a warming Arctic: Arctic climate impact assessment*. Cambridge University Press, Cambridge, 2005.

[2] IPCC, *Climate Change 2007: The Physical Science Basis. Contribution of Working Group I to the Fourth Assessment Report of the Intergovernmental Panel on Climate Change*. S. Solomon, D. Qin, M. Manning, Z. Chen, M. Marquis, K.B. Averyt, M. Tignor and H.L. Miller, Eds. Cambridge University Press, Cambridge, United Kingdom and New York, NY, USA, 2007.

[3] K.F. Huemmrich, G. Kinoshita, J.A. Gamon, S. Houston, H. Kwon, and W.C. Oechel, "Tundra Carbon Balance Under Varying Temperature and Moisture Regimes," *Journal of Geophysical Research,* vol. 115, no. G00I02, doi. 10.1029/2009JG001237, 2010.

[4] E.R. Humpreys, and P.M. LaFleur, "Does earlier snowmelt lead to greater CO_2 sequestration in two low Arctic tundra ecosystems?" *Geophysical Research Letters*, vol. 38, no. L09703, doi. L09703, doi:10.1029/2011GL047339, 2011.

[5] M. Jahn, T. Sachs, T. Mansfeldt, and M. Overesch, "Global climate change and its impacts on the terrestrial Arctic carbon cycle with special regards to ecosystem components and the greenhouse-gas balance," *Journal of Plant Nutrition and Soil Science*, vol. 173**,** pp. 627-643, 2010.

[6] M.T. van Wijk, K.E. Clemmensen, G.R. Shaver, M. Williams, T.V. Callaghan, F.S. Chapin, J.H.C. Cornelissen, L. Gough, S.E. Hobbie, S. Jonasson, J.A. Lee, A. Michelsen, M.C. Press, S.J. Richardson, and H. Rueth, "Long-term ecosystem level experiments at Toolik Lake, Alaska, and at Abisko, Northern Sweden:

generalizations and differences in ecosystem and plant type responses to global change," *Global Change Biology*, vol. 10, no. 1, pp. 105-123, 2004.

[7] E.A.G. Schuur, et al. "Vulnerability of permafrost carbon to climate change: Implications for the global carbon cycle," *BioScience,* vol. 58, no. 8, pp. 701–714, 2008.

[8] L.L. Tieszen, P.C. Miller, and W.C. Oechel, "Photosynthesis," in *An arctic ecosystem: The coastal tundra at Barrow, Alaska*, J. Brown, P.C. Miller, L.L. Tieszen, and F.L. Bunnell, Eds. Dowden, Hutchinson, and Ross, Inc. Stroudsberg. pp. 120-139, 1980.

[9] L. Kappen, "Response to extreme environments," in *The Lichens*, V. Ahmadjian and M.E. Hale, Eds. Academic Press, New York, pp. 311-380, 1974.

[10] D.H.S. Richardson, "Photosynthesis and carbohydrate movement," in *The Lichens*, V. Ahmadjian and M.E. Hale, Eds. Academic Press, New York, pp. 251-288, 1974.

[11] K.A. Kershaw, "Photosynthetic capacity changes in lichens and their potential ecological significance." in *Lichen Physiology and Cell Biology*, D.H. Brown Ed. Plenum Press, New York, pp. 93-109, 1984.

[12] J.H.C.Cornelissen, T.V. Callaghan, J.M. Alatalo, A. Michelsen, E. Graglia, A.E. Hartley, "Global change and Arctic ecosystems: Is lichen decline a function of increases in vascular plant biomass?" *Journal of Ecology*, vol. 89, pp. 984–994, 2001.

[13] A. Hope and D. Stow, "Shortwave Reflectance Properties of Arctic Tundra," in *Landscape Function and Disturbance in Arctic Tundra*, J. Reynolds and J. Tenhuenen Eds. Ecological Studies, Vol. 120. Heidelberg: Springer-Verlag, 1995.

[14] W.G. Rees, O.V. Tutubalina, and E.I. Golubeva, "Reflectance spectra of subarctic lichens between 400 and 2400 nm," *Remote Sensing of Environment*, vol. 90, pp. 281–292, 2004.

[15] D.E. Petzold D.E. and S.N. Goward, "Reflectance spectra of subarctic lichens," *Remote Sensing of Environment*, vol. 24, pp. 481-492, 1988.

[16] J.E. Vogelmann and D.M. Moss, "Spectral reflectance measurements in the genus Sphagnum," *Remote Sensing of Environment*, vol. 45, pp. 273-279, 1993.

[17] I. Olthof and R. Latifovic, "Short-term response of arctic vegetation NDVI to temperature anomalies," *International Journal of Remote Sensing*, vol. 28, pp. 4823–4840, 2007.

[18] I. Olthof and D. Pouliot, "Treeline vegetation composition and change in Canada's western Subarctic from AVHRR and canopy reflectance modeling," Remote Sensing of Environment, vol. 114, no. 4, pp. 805–815, 2010.

[19] S.L. Ustin and J.A. Gamon, "Remote sensing of plant functional types," *New Phytologist*. vol. 186, pp. 795–816, 2010.

[20] J. Brown, K.R. Everett, P.J. Webber , S.F. MacLean Jr, and D.F. Murray, "The coastal tundra at Barrow," in *An Arctic Ecosystem, The Coastal Tundra at Barrow, Alaska*, J. Brown, P.C. Miller, L.L. Tieszen and F.L. Bunnell, Eds. Dowden, Hutchison, and Ross, Stroudsberg, Pennsylvania, pp. 1-29, 1980.

[21] K.M. Hinkel, F.E. Nelson, A.E. Klene and J.H. Bell, "The Urban heat island in winter at Barrow, Alaska," *International Journal Of Climatology*, vol. 23, pp. 1889–1905, 2003.

[22] L.C. Bliss, "The evolution and characteristics of tundra," in *Tundra Ecosystems: a Comparative Analysis*, L.C. Bliss, O.W. Heal and J.J. Moore, Eds. Cambridge University Press, Cambridge, pp. 5-46, 1981.

[23] Webber P.J., Miller P.C., Chapin F.S. III, and McCown B.H. 1980. The Vegetation: pattern and succession, in An arctic ecosystem, The coastal tundra at Barrow, Alaska (eds Brown J., Miller P.C., Tieszen L.L., and Bunnell F.L.), Dowden, Hutchison, and Ross, Stroudsberg, Pennsylvania: 186-218

[24] F.E. Wielgolaski, L.C. Bliss, J. Svoboda, and G. Doyle, "Primary production of tundra," in *Tundra Ecosystems: a Comparative Analysis*, L.C. Bliss, O.W. Heal and J.J. Moore, Eds. Cambridge University Press, Cambridge, pp. 187-225, 1981.

[25] D.A. Stow, A. Hope, D. McGuire, et al. "Remote sensing of vegetation and land-cover change in Arctic tundra ecosystems," *Remote Sensing of Environment*, vol. 89, pp. 281-308, 2004.

[26] K.F. Huemmrich, J.A. Gamon, C.E. Tweedie, S.F. Oberbauer, et al. "Remote sensing of tundra gross ecosystem productivity and light use efficiency under varying temperature and moisture conditions," *Remote Sensing of Environment*, vol. 114, no. 3, pp. 481-489, 2010.

[27] J.A. Gamon, Y. Cheng, H. Claudio, L. MacKinney, and D. Sims, "A mobile tram system for systematic sampling ecosystem optical properties," *Remote Sensing of Environment*, vol. 103, pp. 246-254, 2006.

[28] S.G. Ungar, J.S. Pearlman, J.A. Mendenhall, and D. Reuter, "Overview of the Earth Observing One (EO-1) mission," *IEEE Transactions on Geoscience and Remote Sensing*, vol. 41, no. 6, pp. 1149-1159, 2003.

[29] B.-C. Gao, K.B. Heidebrecht, and A.F.H. Goetz, "Derivation of scaled surface reflectances from AVIRIS data," *Remote Sensing of Environment,* vol. 44, pp. 165-178, 1993.

[30] B.-C. Gao, M.J. Montes, C.O. Davis, and A.F.H. Goetz, "Atmospheric correction algorithms for hyperspectral remote sensing data of land and ocean," *Remote Sensing of Environment*, vol. 113, Supplement 1, pp. S17-S24, 2009.

[31] W.R. Klecka, *Discriminant Analysis*, Sage Publications, Inc., Newbury Park, CA, USA, 1980.

[32] A.A. Gitelson, G.P. Keydan, and M.N. Merzlyak, "Three-band model for non-invasive estimation of chlorophyll, carotenoids, and anthocyanin contents in higher plant leaves," *Geophysical Research Letters*, vol. 33, pp. L11402, 2006.

[33] S.L. Ustin, A.A. Gitelson, S. Jacquemoud, M. Schaepman, G.P. Asner, J. A. Gamon, and P. Zarco-Tejada, "Retrieval of foliar information about plant pigment systems from high resolution spectroscopy," *Remote Sensing of Environment*, vol. 113, pp. S67–S77, 2009.

[34] A.A. Gitelson, "Nondestructive estimation of foliar pigment (chlorophylls, carotenoids, and anthocyanins) contents: Evaluating a semianalytical three-band model" in *Hyperspectral Remote Sensing of Vegetation*, P.S. Thenkabail, J.G. Lyon, and A. Huete, Eds. Taylor and Francis, 2011.

[35] T. Mulhern, "Spectral contrasts of subarctic vegetation: basis for mapping lichens with satellite data," PhD dissertation, University of Maryland at College Park, 1995.

[36] L.C. Smith, Y. Sheng, G.M. MacDonald, and L.D. Hinzman," Disappearing Arctic lakes." *Science*, vol. 308, pp. 1429, 2005.

[37] C. Roberto, B. Lorenzo, M. Michele, R. Micol, and P. Cinzia, "Optical remote sensing of vegetation water content" in *Hyperspectral Remote Sensing of Vegetation*, P.S. Thenkabail, J.G. Lyon, and A. Huete, Eds. Taylor and Francis, 2011.

[38] S. Goswami, J.A. Gamon, and C.E. Tweedie, "Surface hydrology of an arctic ecosystem: multi-scale analysis of a flooding and draining experiment using spectral reflectance," J. *Geophys. Res.*, vol. 116, no. G00I07, doi 10.1029/2010JG001346, 2010.

[39] M. Sturm, C. Racine, and K. Tape, "Increasing shrub abundance in the Arctic," *Nature*, vol. 411, pp. 546-547, 2001.

Table Captions

Table 1. Light Use Efficiency based on regressions between net photosynthesis and APAR from plot data. LUE is in units of mol CO_2 mol^{-1} absorbed quanta.

Table 2. Description of relationships in spectral space between the statistical distance to endmembers and coverage estimate observations, acquired along the tram transect. The errors are expressed in percent coverage. For all cases the number of observations is 100.

	Vascular Plants	Moss	Lichen
LUE	0.01337	0.00184	0.00124
St. Err. of Slope	0.00101	0.00022	0.00011
Num. Obs.	29	25	28
R^2	0.74	0.56	0.74
P	<0.01	<0.01	<0.01

Table 1.

	Vascular Plants	Moss	Lichen
R^2	0.39	0.13	0.19
P	<0.01	<0.01	<0.01
Est. Obs. Error	9.5	7.1	7.0
SE of Regression	10.8	8.4	9.0

Table 2.

Figure Captions

Figure 1. Absorbed PAR and gross photosynthesis for the three vegetaton functional types from plot data collected July 20 and August 5, 2001. Light use efficiency for each functional type was calculated from these data as the slope forced through the origin.

Figure 2. Endmember spectral reflectance for each cover type, vertical lines indicate wavelengths used in the DA.

Figure 3. The distribution of data from plots using the first two functions derived from DA for the three vegetation functional types and nongreen materials. The larger gray circles indicate values used as endmembers in the unmixing analysis.

Figure 4. Observed variation in coverage at 1 m intervals along the transect, visually estimated over the period August 8-11, 2001. Because the vegetation is 3-dimentional, total cover fractions were over 100%. In the data analysis the total cover fractions were normalized to equal 100%.

Figure 5. LUE along the 100 m transect shown with the black line was estimated from the functional type coverage (shown in Figure 4) and light use efficiency (shown in Figure 1), along with LUE estimated using coverage derived from spectral data shown with the gray line. Microtopography is shown as dashed line. Error in Observed LUE estimate is

0.00136 mol C mol^{-1} quanta, RMSE in LUE derived from observations compared to LUE from spectra is 0.00266 mol C mol^{-1} quanta.

Figure 6. Comparison between observed vegetation functional type coverage normalized to 100% for vascular plants, mosses, and lichens along the transect and cover fractions estimated from spectral reflectance. Line is 1 to 1 line. The absolute error in visual estimates is approximately 9%. The RMSE of spectral retrievals is 9% absolute.

Figure 7. LUE (mol C mol^{-1} quanta) along the transect estimated based on observed normalized cover fractions and cover fractions obtained from spectral unmixing. Line is 1 to 1 line. Errors in LUE based on observed cover fractions are due to errors in LUE for the pure functional types and an assumed 15% error of observed raw coverage amounts. Errors in LUE based on spectrally derived cover fractions are due to errors in LUE for pure functional types and the RMSE of the spectral retrieval of cover fractions.

Figure 8. Three versions of the EO-1 Hyperion image acquired on July 20, 2009 are shown.
Left: 3-band (RGB=834, 671, and 549 nm) composite image of surface reflectance. The grid of light blue lines on the lower left side of the image is the city of Barrow. The straight blue line along the shore near the top of the image is the old airport runway. The oblong features are drained thermokarst lakes and the dark red ones are now marshes.

Middle: Three band RGB continuous fields of estimated coverage of vegetation functional types derived from spectral unmixing and scaled between 0 and 100% coverage. R = Vascular Plant Cover, G = Moss Cover, B = Lichen Cover

Right image: Map of LUE spatial patterns (mol C mol^{-1} quanta x1000) based on coverage estimates.

Figure 9. Scatter plot of chlorophyll index (x-axis) versus LUE (mol C mol^{-1} quanta x1000) based on normalized cover fractions (y-axis). Both variables were retrieved from the Hyperion image.

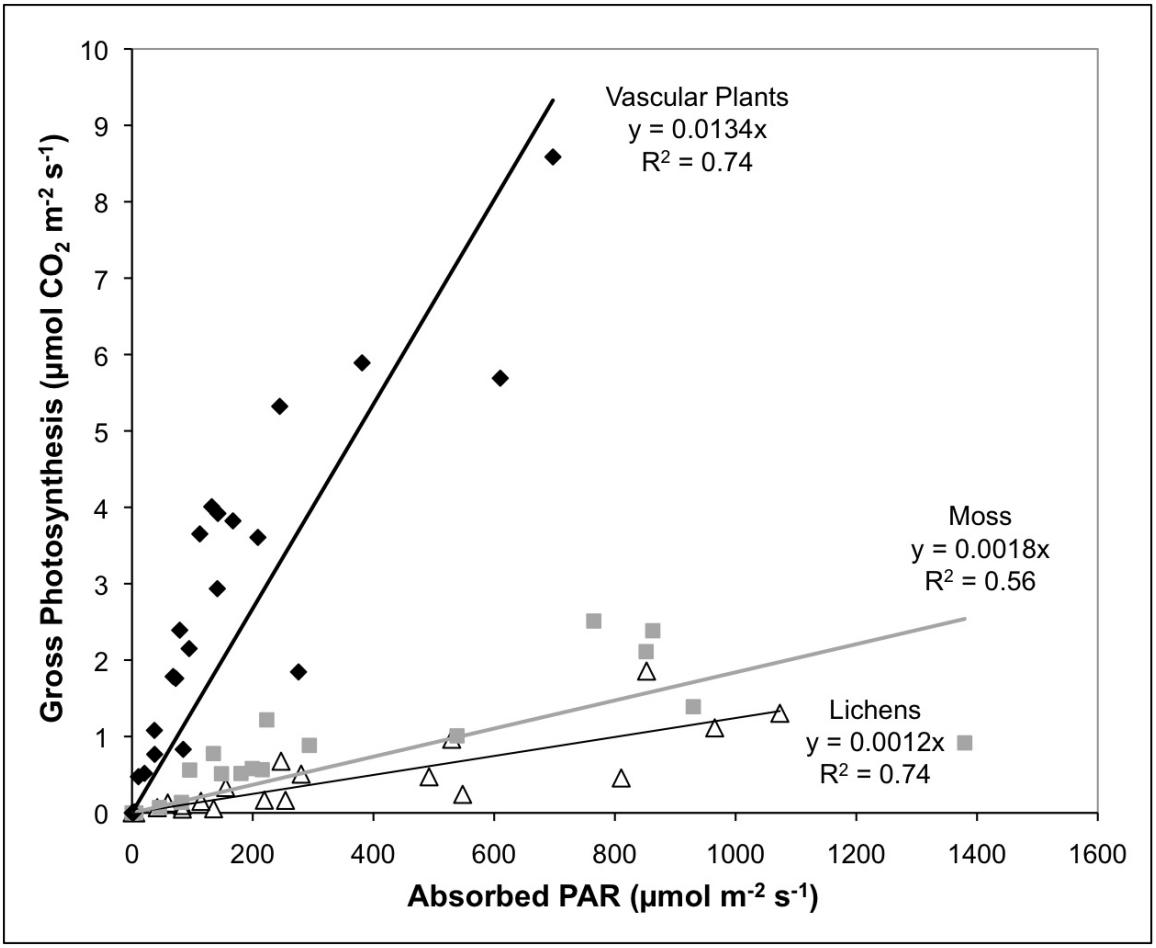

Figure 1.

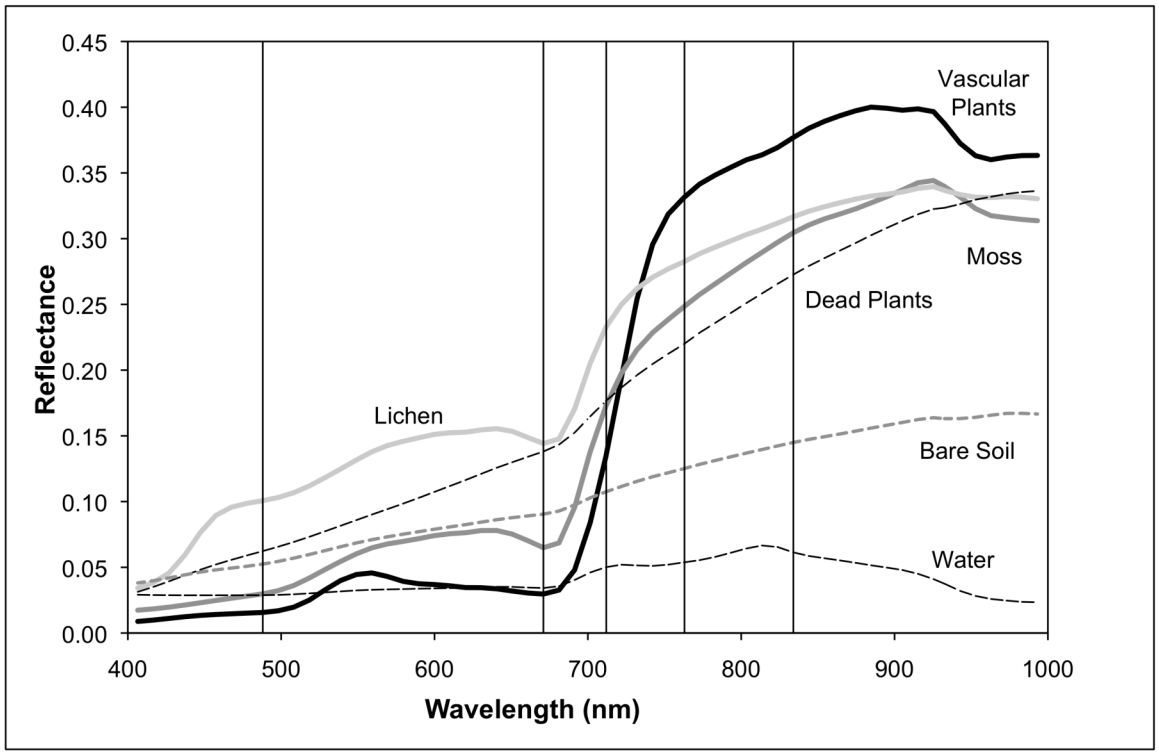

Figure 2.

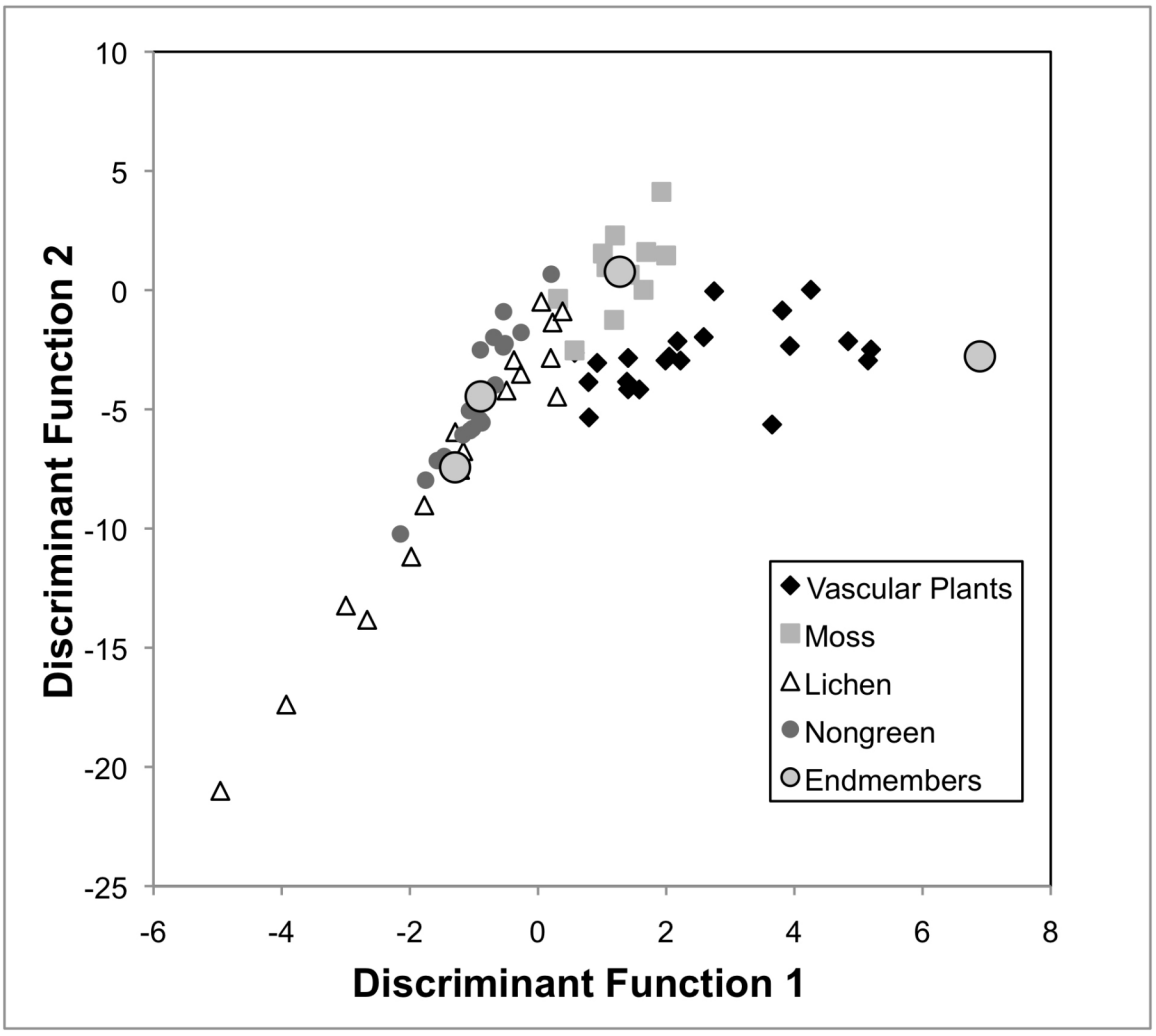
Discriminant Function 2
Discriminant Function 1
10
5
0
-5
-10
-15
-20
-25
-6
-4
-2
0
2
4
6
8
Vascular Plants
Moss
Lichen
Nongreen
Endmembers

Figure 3.

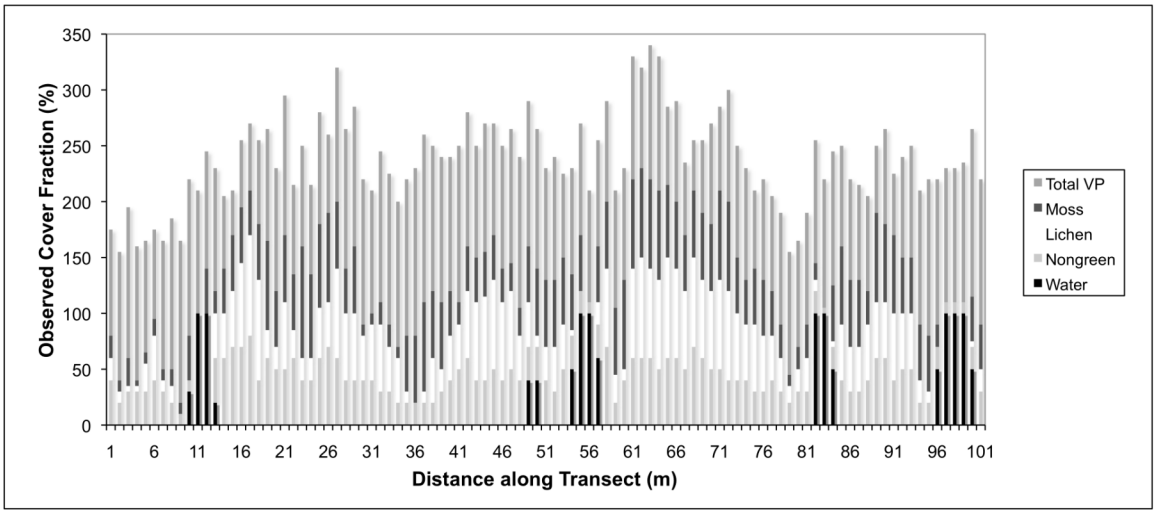
Observed Cover Fraction (%)
Distance along Transect (m)
350
300
250
200
150
100
50
0
1
6
11
16
21
26
31
36
41
46
51
56
61
66
71
76
81
86
91
96
101
Total VP
Moss
Lichen
Nongreen
Water

1 Figure 4.

2

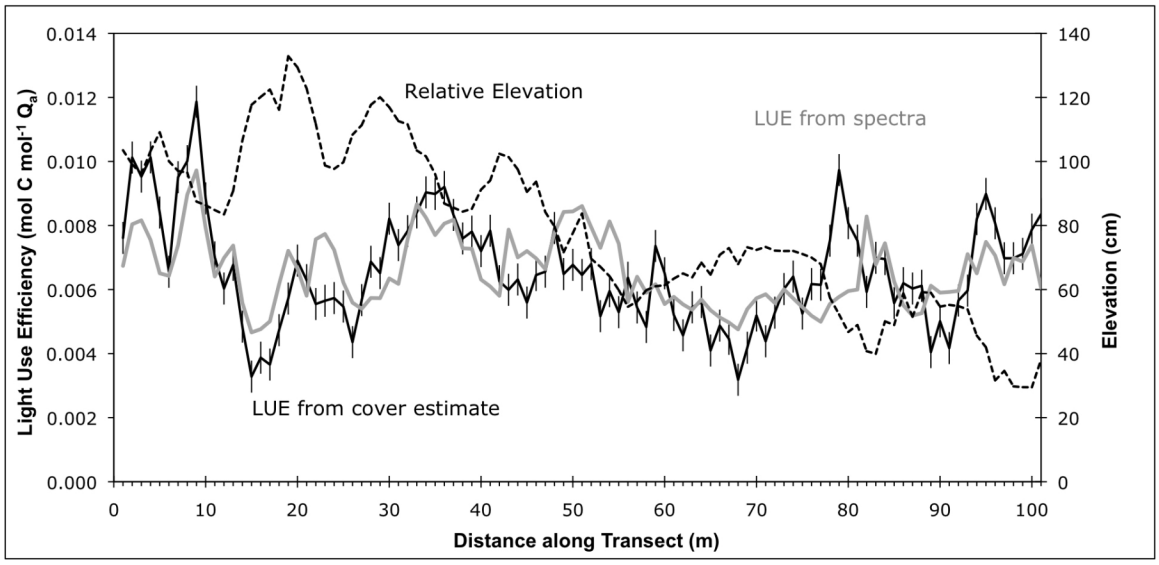

3

4 Figure 5.

5

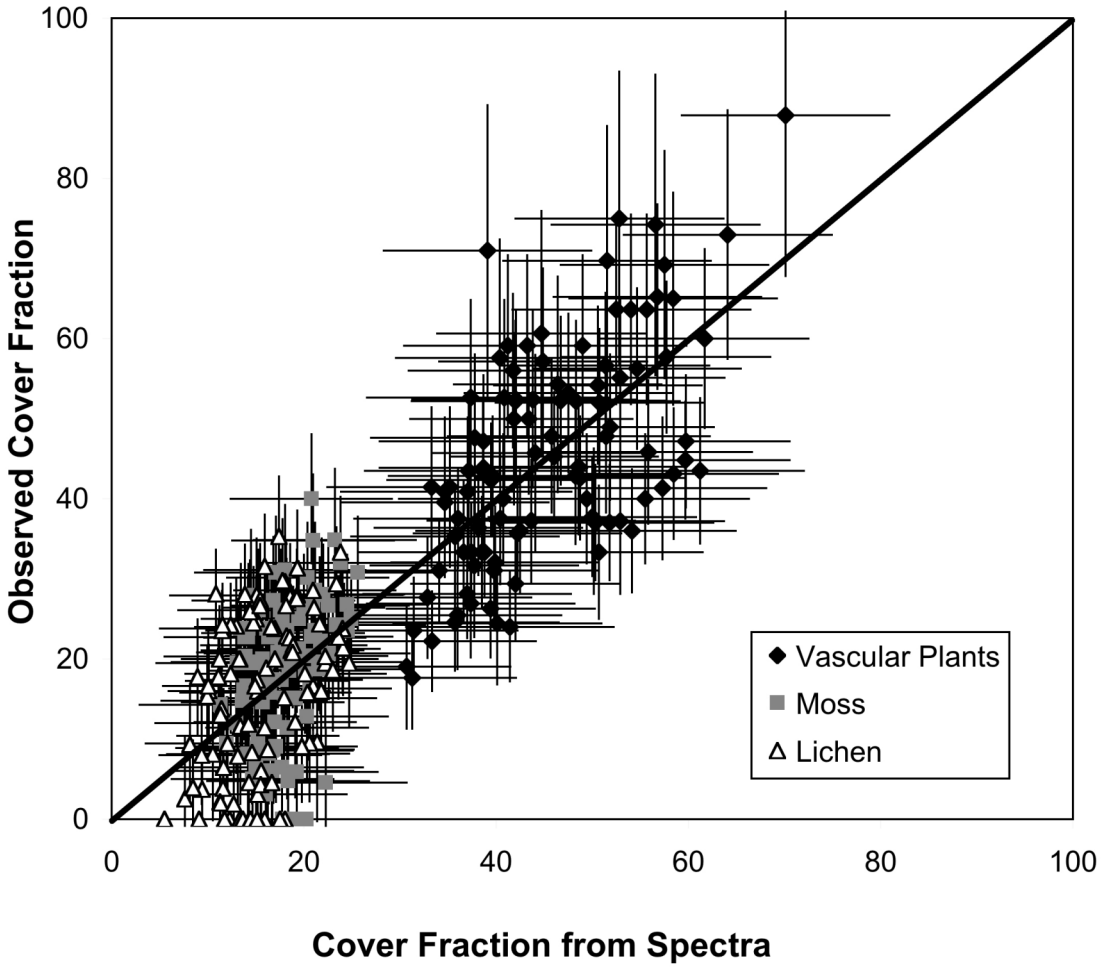
Observed Cover Fraction
Cover Fraction from Spectra
0
20
40
60
80
100
Vascular Plants
Moss
Lichen

Figure 6.

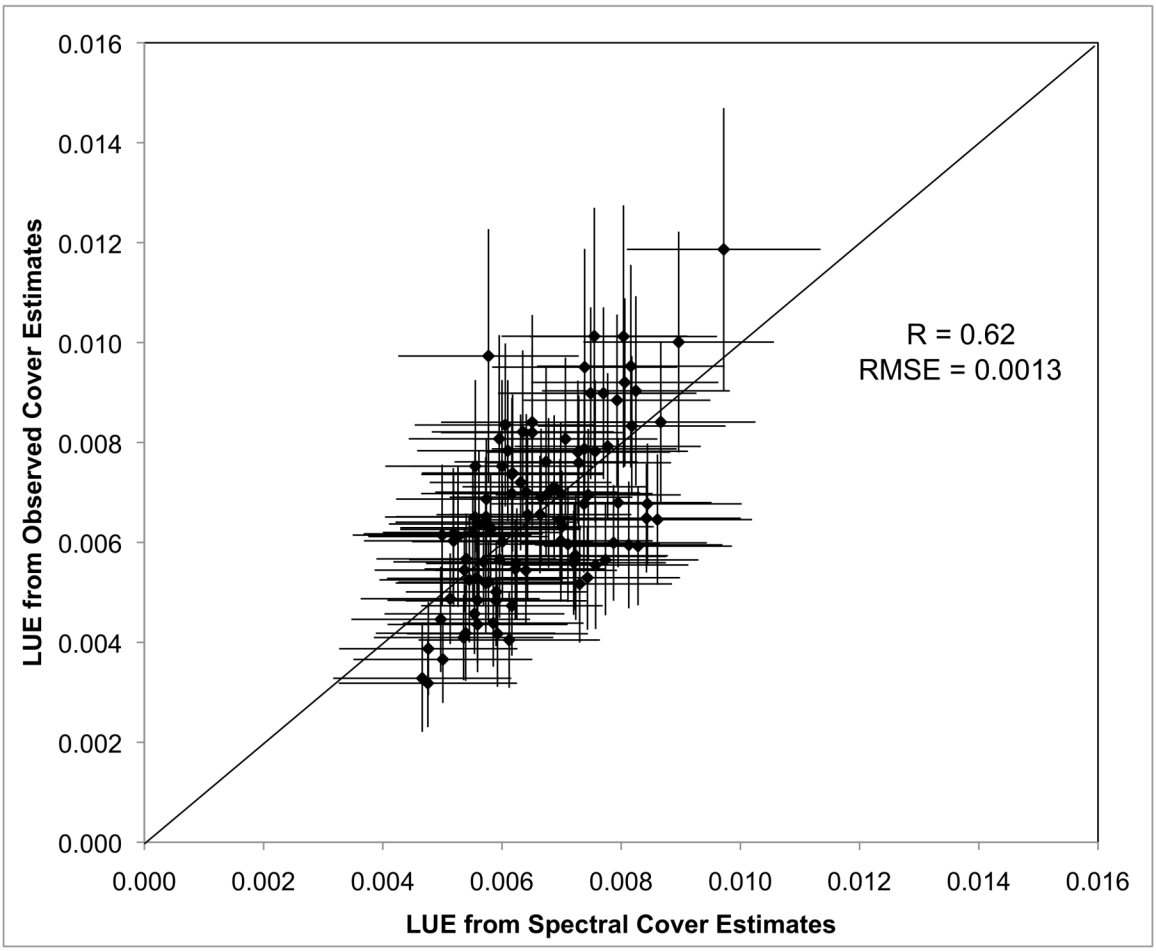
0.016
0.014
0.012
0.010
0.008
0.006
0.004
0.002
0.000
LUE from Observed Cover Estimates
0.000
0.002
0.004
0.006
0.008
0.010
0.012
0.014
0.016
LUE from Spectral Cover Estimates
R = 0.62
RMSE = 0.0013

Figure 7.

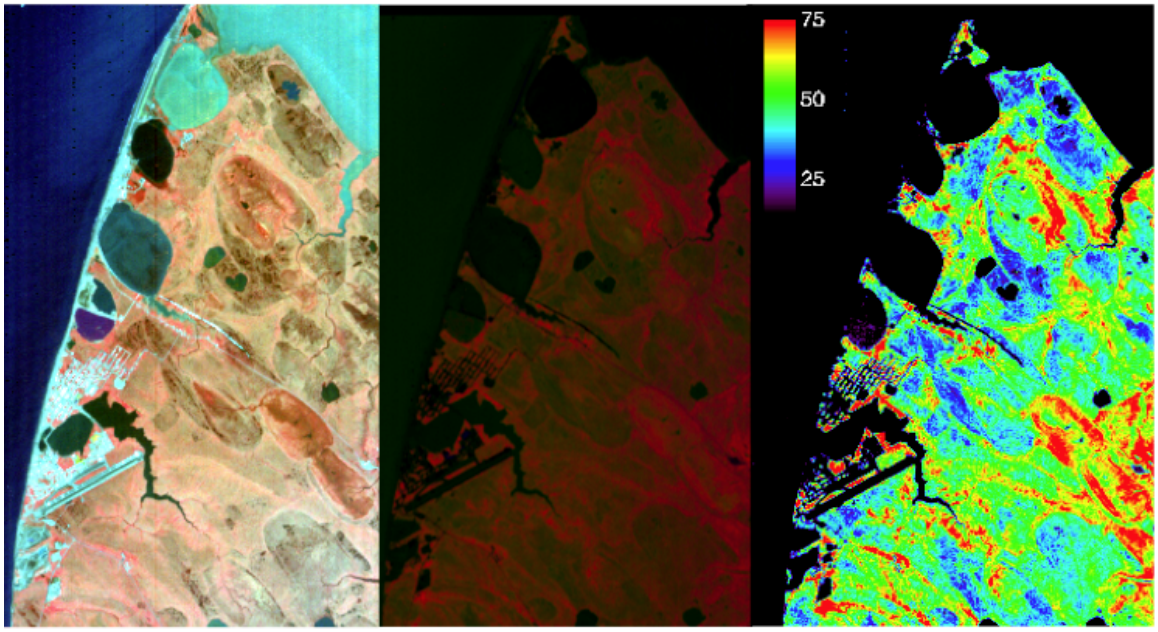

Figure 8.

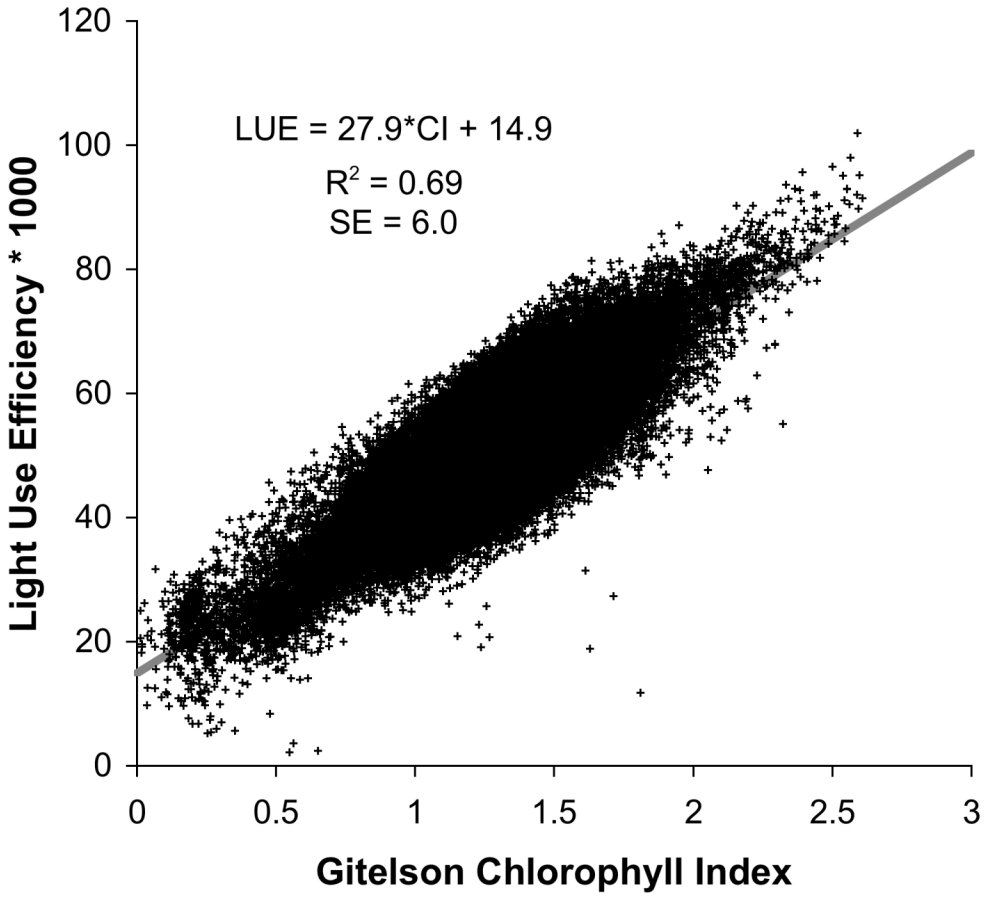
LUE = 27.9*CI + 14.9
R2 = 0.69
SE = 6.0
Light Use Efficiency * 1000
Gitelson Chlorophyll Index
0
20
40
60
80
100
120
0
0.5
1
1.5
2
2.5
3

Figure 9.